Delay in Atomic Photoionization

A. S. Kheifets[1,2,*] and I. A. Ivanov[1]

[1]Research School of Physical Sciences, The Australian National University, Canberra ACT 0200, Australia
[2]The Kavli Institute for Theoretical Physics, University of California, Santa Barbara, California 93106-4030, USA

(Received 13 October 2010; published 1 December 2010)

We analyze the time delay between emission of photoelectrons from the outer valence ns and np subshells in noble gas atoms following absorption of an attosecond extreme ultraviolet pulse. Various processes such as elastic scattering of the photoelectron on the parent ion and many-electron correlation affect the apparent ''time zero'' when the photoelectron leaves the atom. This qualitatively explains the time delay between photoemission from the $2s$ and $2p$ subshells of Ne as determined experimentally by attosecond streaking [Science **328**, 1658 (2010)]. However, with our extensive numerical modeling, we were only able to account for less than half of the measured time delay of 21 ± 5 as. We argue that the extreme ultraviolet pulse alone cannot produce such a large time delay and it is the streaking IR field that is most likely responsible for this effect.

DOI: 10.1103/PhysRevLett.105.233002 PACS numbers: 32.30.Rj, 31.15.ve, 32.70.−n, 32.80.Fb

Among other spectacular applications of the attosecond streaking technique, it has become possible to determine the time delay between subjecting an atom to a short laser pulse and subsequent emission of the photoelectron. In a recent work by Eckle *et al.* [1], the helium atom was subjected to a near-infrared laser pulse with an intensity of several units of 10^{14} W/cm^2. Such a strong field ionization regime could be characterized by a fairly small Keldysh parameter $\gamma \simeq 1$. The time delay in such a photoemission process can be conveniently analyzed in terms of nonadiabatic tunneling [2]. In a subsequent experiment by Schultze *et al.* [3], the time delay was measured in neon in the extreme ultraviolet (XUV) photon energy range by high-order harmonic conversion of the driving near-infrared laser pulse. In this regime, which is characterized by a moderate intensity, short wavelength, and $\gamma \gg 1$, it is believed that the formation of the outgoing wave packet follows instantaneously temporal variation of the incident electromagnetic field. Nevertheless, a sizable time delay of 21 ± 5 as was reported between photoemission from the $2s$ and $2p$ valence subshells of Ne. Schultze *et al.* [3] argued that a comprehensive temporal characterization of photoemission on the attosecond time scale could provide a new insight into intra-atomic electron correlations. Indeed, the best theoretical treatment within an independent electron model could only account for 4.0 as time delay. When the theoretical model was corrected for electron correlations before and after photoionization, a relative delay of 6.4 as was obtained. This unresolved difference between the measured and calculated time delays puts many-electron models of atomic photoionization under significant strain. If substantiated, this difference could potentially point to new physical mechanisms underpinning electromagnetic interaction in atoms on the attosecond time scale.

In this Letter, we perform an extensive study of the time delay between the ns^2 and np^6 outer valence subshell photoionization in noble gas atoms. We employ both the explicit time-dependent and stationary treatments of the photoionization process. To this end, we solve the time-dependent Schrödinger equation (TDSE) in the single active electron approximation. By carefully examining the time evolution of the photoelectron wave packet, we establish the apparent ''time zero'' when the photoelectron leaves the atom. To account for electron correlation, we solve a set of coupled integral equations in the random phase approximation with exchange (RPAE) [4].

Within an independent electron approximation, the time delay is caused by the energy dependence of the elastic scattering phase shifts of the photoelectron moving in the Hartree-Fock (HF) potential of the Ne^+ ion. The many-electron correlation, which is due to intershell $2s$-$2p$ coupling, depends on the energy of the photon and thus adds an additional component to the quantum phase of the dipole matrix element. Both these effects account for the time delay not exceeding $\sim$10 as. This recovers only about one-half of the experimental value of 21 ± 5 as. We carefully examine other correlation and polarization corrections but find them unable to produce any sizable contribution to the measured time delay. We also analyze these effects in other noble gas atoms.

The time-dependent calculation of photoionization in Ne was performed by radial grid integration of the TDSE using the matrix iteration method [5]. We employed a one-electron basis in a parametrized optimized effective potential [6]. We used the linearly polarized XUV pulse $\mathcal{E}(t) = E_0 g(t) \cos\omega t$ with the envelope $g(t)$ represented by the Nutall window function and centered at $t = 0$. The following field parameters were chosen: $E_0 = 0.119$ a.u. (corresponding to the peak intensity of 5×10^{14} W/cm^2), $\omega = 106$ eV, $T = 2\pi/\omega = 39$ as, and FWHM $= 182$ as. Experimental field intensity was not reported by Schultze *et al.* [3]. Given a typical high-order harmonic conversion

efficiency of 10^{-6} [7], the presently chosen XUV field strength is most certainly larger than the one used experimentally. With this choice, our calculation is guaranteed to account for nonperturbative, with respect to the field, ionization effects if these effects were to be sizable. Other XUV field parameters used in the present work were identical to those used in the experiment. The XUV pulse described above is shown in the top panel of Fig. 1 (dotted black line). The pulse is truly off outside the interval $\pm T_1$, where $T_1 \simeq 5T$, which is about twice the FWHM.

The solution of the TDSE satisfies the initial condition $\Psi(\boldsymbol{r}, t = T_1) = \phi_i(\boldsymbol{r})$, which corresponds to a bound electron state on the atomic shell i to be ionized. So the shell index i is implicit in the following but omitted for brevity. The wave packet representing the photoelectron ejected from a given shell is defined as

$$\Phi(\boldsymbol{r}, t) = \sum_L \int a_{kL}(t)\chi_{kL}(\boldsymbol{r})e^{-iE_k t}dk, \qquad (1)$$

where $a_{kL}(t) = e^{iE_k t}\langle\chi_{kL}|\Psi(t)\rangle$ are the projection coefficients of the solution of the TDSE on the continuum spectrum of the atom. The continuum state $\chi_{kL}(\boldsymbol{r}) = R_{kl}(r)Y_L(\boldsymbol{r}/r)$ is the product of the radial orbital with the asymptotic $R_{kl} \propto \sin[kr + \delta_l(k) + (1/k)\ln(2kr) - l\pi/2]$ and the spherical harmonic $Y_L(\boldsymbol{r}/r)$ with $L \equiv l, m$. The projection coefficients $a_{kl}(t)$ cease to depend on time for $|t| > T_1$ when the driving XUV pulse is off.

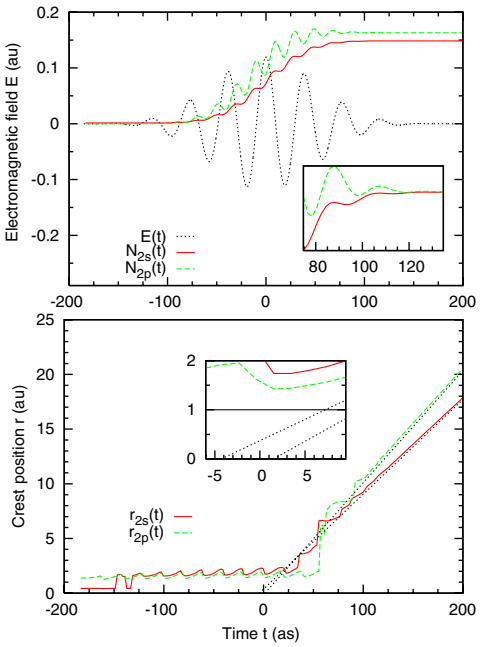

FIG. 1 (color online). Top: The norm of the wave packets $N(t)$ (scaled arbitrarily) emitted from the $2s$ and $2p$ subshells is plotted as a function of time with the red solid and green dashed lines, respectively. The XUV pulse is overplotted with the black dotted line. In the inset, the norm variation $[N(t) - N(T_1)]/N(T_1)$ is shown on an expanded time scale near the pulse end. Bottom: The crest position of the $2s$ and $2p$ wave packets is shown with the same line styles. The crest position after the pulse end is fitted with the straight line, which corresponds to the free propagation. In the inset, extrapolation of the free propagation inside the atom is shown.

There are two convenient indicators of the evolution of the wave packet (1). One is the norm given by the integral $N(t) = \sum_L \int dk|a_{kL}(t)|^2$. This norm is plotted in the top panel of Fig. 1 with the red solid and green dashed lines for the wave packets that originated from the $2s$ and $2p$ subshells, respectively. For better clarity, these curves are scaled and overplotted on the electromagnetic pulse.

The figure shows clearly that the evolution of the $2s$ and $2p$ wave packets starts and ends at the same time without any noticeable delay. This is further visualized in the inset, where the variation of the norm $[N(t) - N(T_1)]/N(T_1)$ is plotted on an expanded time scale near the driving pulse end. Indeed, the norm starts deviating from zero with the rise of the XUV pulse and reaches its asymptotic value once the interaction with the XUV pulse is over.

Another marker of the wave packet dynamics is the crest position, defined as a location of the global maximum of the electron density. The latter quantity is truly informative only when the electron is outside the atom and the wave packet is fully formed, having one well-defined global maximum. In the bottom panel of Fig. 1, we show the crest position of the $2s$ and $2p$ wave packets propagating in time. This figure can be viewed as a more realistic version of a somewhat idealized and simplified graph presented in Fig. 1 of Schultze *et al.* [3]. We see that evolution of the norm and the movement of the crest commence and cease at about the same time.

The movement of the crest becomes almost linear when the norm reaches its asymptotic value and the wave packet is fully formed. Once fitted with the linear time dependence $r = k(t - t_0) + r_0$ for large times $t > T_1$ (shown as a dotted straight line) and backpropagated inside the atom, the $2s$ wave packet seems to have an earlier start time t_0 than that of the $2p$ wave packet. This difference is magnified in the inset. It is about 6 as at the origin $r_0 = 0$ and about 4 as at the distance $r_0 \sim 1$ au, which corresponds to the size of the valence shell of the Ne atom. We see that at the origin $t_0^{2s} < 0$ and $t_0^{2p} > 0$ are shifted to the opposite direction with respect to the peak of the driving XUV pulse which sets the start time of the photoionization process. Thus the seeming (or apparent according to Ref. [3]) time zero of the wave packet, which is inferred by the backward time propagation, is different from the physical (or real) time zero $t = 0$.

The origin of this shift is most clearly elucidated within the perturbation theory framework, which should be applicable under the present field conditions of a single photon transition with $\gamma \gg 1$ [8]. Under these conditions,

$$a_{kL}(t > T_1) = -i\int_{-\infty}^{\infty} \langle\chi_{kL}|z|\phi_i\rangle e^{i(E_k - \epsilon_i)\tau}\mathcal{E}(\tau)d\tau. \qquad (2)$$

Here we extended the integration limits outside the pulse duration and wrote the dipole matrix element $\langle \chi_{kL}|z|\phi_i\rangle$ in the length gauge. By separating the angular and radial integration, we can present this matrix element in the reduced form

$$\langle \chi_{kL}|z|\phi_i\rangle \propto C^{lm}_{10l_im_i} d_\lambda(k), \tag{3}$$

where $C^{lm}_{10l_im_i}$ is the Clebsch-Gordan coefficient, $\lambda \equiv l, i$, and $d_\lambda(k)$ is real. With this definition, we can write $a_{kL} \propto -id_\lambda(k)\tilde{\mathcal{E}}(E_k - \epsilon_i)$, where the Fourier transform of the XUV field $\tilde{\mathcal{E}}(\omega) = \int_{-\infty}^{\infty} e^{i\omega\tau}\mathcal{E}(\tau)d\tau$ is real for a symmetric pulse that we presently consider. We note that Eqs. (1)–(3) are equivalent to Eqs. (S5)–(S8) of Schultze *et al.* [3] given in their supporting online material.

To describe the motion of the wave packet (1), we apply the usual saddle-point method. For each l, the crest of the wave packet is moving at large times $t > T_1$ quasiclassically along the trajectory which is given by the equation

$$r = k\left\{t - \frac{d}{dE}\left[\delta_l(k) + \frac{1}{k}\ln(2kr)\right]_{k=\sqrt{2E_0}}\right\}. \tag{4}$$

Since the logarithm is a slowly varying function which can be absorbed into a constant, Eq. (4) describes a straight line: $r = k(t - t_0) + r_0$, with $t_0 = d\delta_l(k)/dE|_{k=\sqrt{2E_0}}$. Thus the relative time delay between various photoionization channels is determined primarily by the derivatives of the corresponding elastic scattering phases [9].

The scattering phases $\delta_l(k)$ of the photoelectron moving in the field of a singly charged Ne^+ ion are shown in the middle panel of Fig. 2. The photoelectron ejected from the $2s$ shell has only one value of the angular momentum $l = 0$, whereas the $2p$ photoelectron can acquire two angular momenta $l = 0$ and 2. The phases in the s and p waves are shifted downwards by π and $\pi/2$, respectively, for better clarity. In the top panel of the same figure, we display the asymptotic projection coefficients $a_L(k)$ for $l = 0$, 1, and 2 and $m = 0$. The centers of the energy distribution of the l-projected coefficients (indicated by the vertical dotted lines in the top panel) define the position of the energy derivative of the corresponding scattering phases $d\delta_l(k)/dE|_{k=\sqrt{2E_0}}$ (indicated by the straight lines in the middle panel). We see that the energy derivatives of the s and p phases are negative, whereas that of the d phase is positive. This is so due to the presence of the occupied s and p states in the Ne^+ ion which disturbs the otherwise monotonic increase with energy of the Coulomb phase (the Levinson-Seaton theorem [10]). Because the $2p \rightarrow kd$ transition is strongly dominant over the $2p \rightarrow ks$ one, as is seen from the corresponding projection coefficients in the top panel of Fig. 2, it is the d phase that determines the shift of the apparent time zero of the $2p$ wave packet relative the physical time zero $t = 0$. This shift is positive for the $2p$ wave packet and negative for the $2s$ one, in accordance with our observation displayed in the inset of the bottom panel of Fig. 1.

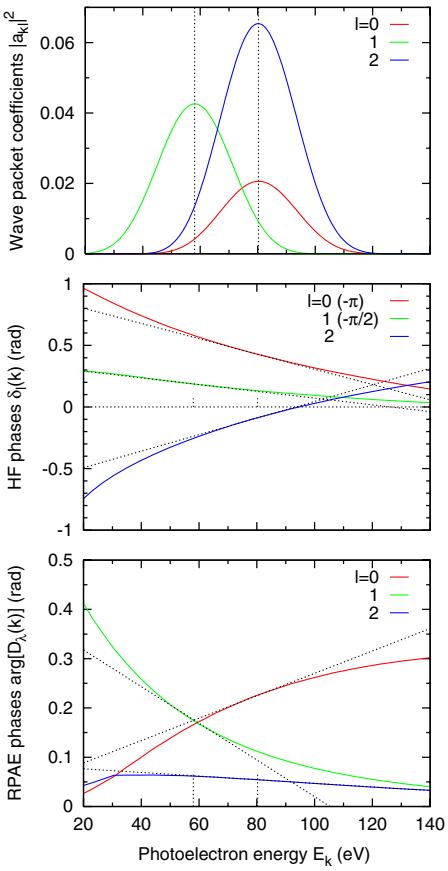

FIG. 2 (color online). Top: Expansion coefficients $|a_{kl}|^2$ plotted versus the photoelectron energy $E_k = k^2/2$, which is expressed in eV. Middle: The HF scattering phases. Bottom: Phases of the RPAE dipole matrix elements $\arg[D_\lambda(k)]$.

So far, we confined ourselves with an independent electron approximation and calculated the dipole matrix elements $d_\lambda(k)$ and the scattering phases $\delta_l(k)$ in the HF approximation [11,12]. It is well known, however, that many-electron correlation modifies strongly the dipole matrix elements. The full account for this effect can be taken within the RPAE model [4] by solving a set of coupled integral equations:

$$D_\lambda(k) = d_\lambda(k) + \sum_\nu \int dp D_\nu(p)\chi_\nu(p)U_{\nu\lambda}(p,k). \tag{5}$$

Here $\chi_\nu(p) = (\omega - E_p - \epsilon_\nu + i\epsilon)^{-1}$ is the Green's function, and $U_{\nu\lambda}(p,k)$ is the Coulomb interaction matrix. The one-electron HF basis corresponding to the field of the singly charged Ne^+ ion accounts for direct photoelectron interaction with its parent shell. It is therefore the intershell Coulomb interaction with $\nu \neq \lambda$ that should only be included into Eq. (5). Since the Green's function is complex, the dipole matrix elements $D_\lambda(k)$ acquire an additional phase, which is plotted in the bottom panel of Fig. 2.

The HF phase derivatives alone account for the apparent time zero shift between the $2s$ and $2p$ ionization $\Delta t_0^{2s-2p} = 6.2$ as. The RPAE correction adds an extra 2.2 as. In total, this accounts for the apparent time zero shift

$\Delta t_0^{2s-2p} = 8.4$ as. Both the HF and RPAE phases are smooth functions of the photoelectron energy, and their averaging over the bandwidth of the XUV pulse does not change these numbers in a noticeable way. The analogous values reported by Schultze *et al.* [3] for the independent electron model and the correlation correction are 4.0 and 2.4 as, respectively. Both sets of calculations are quite close and well below the experimental value of 21 ± 5 as.

One could argue that the complete account for many-electron correlation within the TDSE, rather than adding this correlation *ad hoc*, could modify the present result. This is, however, unlikely given the nature of the RPAE which is a direct generalization of the HF method in the presence of an oscillatory external electromagnetic field [13]. The only approximation taken when deriving Eq. (5) is that at any instant of time the atomic wave function is an antisymmetric product of one-electron functions. It is quite a robust approximation under the field parameters considered above.

We also evaluated the time delay of the wave packet relative to the XUV pulse in other noble gases. In He, the wave packet emitted from the $1s$ shell is delayed by ~ 2 as relative to the center of the XUV pulse. This follows from the independent electron HF calculation, which returns a positive derivative of the p phase shift as there is no occupied p orbital in the He^+ ion. It is also confirmed by the correlated convergent close-coupling model, which is known to produce benchmark photoionization results for He in the XUV range [14]. It is to be compared with 5 as delay reported for He by Schultze *et al.* [3]. In heavier noble gases, Ar and Kr, the difference of the HF p- and d-phase derivatives becomes smaller as occupation of the ionic orbitals increases in line with the Levinson-Seaton theorem. In Kr, the d-phase derivative becomes negative as the $3d$ orbital is occupied. Accordingly, the time delay between the wave packets emitted from the ns and np valence subshells is getting smaller. When the HF and RPAE phase derivatives are combined, it results in 5.8 as delay in Ar and nearly zero delay in Kr around the 100 eV photon energy mark.

In conclusion, we examined various effects leading to the shift between the apparent time zero of the photoelectron wave packets emitted from the $2s$ and $2p$ shells in neon relative to the center of the XUV pulse which sets the timing of the photoionization process. We found that this shift is primarily due to the energy derivative of the HF elastic scattering phase shifts which differs significantly for various partial waves. The RPAE correction, which accounts for many-electron correlation, is rather small and cannot explain the profound difference between the theoretical and experimental time delay.

The apparent time zero is meaningful only when the wave packet is detected at large distances from the atom as in attosecond streaking experiments. This apparent time zero has little to do with the real time when the atomic photoionization begins, which is fully determined by the driving XUV pulse alone. In this sense, the attosecond streaking is not informative on the early stages of the photoionization process. However, this technique allows one to determine the energy derivative of the quantum phase of the dipole matrix element [15], thus facilitating the so-called complete photoionization experiment [16]. This is particularly important in those targets where the many-electron correlation is significant.

The full potential of the attosecond streaking technique and its successful application in atomic collision physics can be realized only if the current strong disagreement between theory and experiment in Ne is resolved. The present study was not able to do so. Our simulations and analytic arguments indicate that the XUV pulse alone cannot produce such a large time delay and it is the streaking IR field that is most likely responsible for this effect.

The authors acknowledge support of the Australian Research Council in the form of Discovery Grant No. DP0771312. Resources of the National Computational Infrastructure (NCI) Facility were employed. One of the authors (A. S. K.) thanks the Kavli Institute for Theoretical Physics for hospitality. This work was supported in part by the NSF Grant No. PHY05-51164

*Corresponding author.
A.Kheifets@anu.edu.au

[1] P. Eckle *et al.*, Science **322**, 1525 (2008).
[2] G. L. Yudin and M. Y. Ivanov, Phys. Rev. A **63**, 033404 (2001).
[3] M. Schultze *et al.*, Science **328**, 1658 (2010).
[4] M. Y. Amusia, *Atomic Photoeffect* (Plenum, New York, 1990).
[5] M. Nurhuda and F. H. M. Faisal, Phys. Rev. A **60**, 3125 (1999).
[6] A. Sarsa, F. J. Gálvez, and E. Buendia, At. Data Nucl. Data Tables **88**, 163 (2004).
[7] E. Goulielmakis *et al.*, Science **320**, 1614 (2008).
[8] N. B. Delone and V. P. Krainov, *Atoms in Strong Light Fields* (Springer-Verlag, Berlin, 1985).
[9] C. A. A. de Carvalho and H. M. Nussenzveig, Phys. Rep. **364**, 83 (2002).
[10] L. Rosenberg, Phys. Rev. A **52**, 3824 (1995).
[11] L. V. Chernysheva, N. A. Cherepkov, and V. Radojevic, Comput. Phys. Commun. **11**, 57 (1976).
[12] L. V. Chernysheva, N. A. Cherepkov, and V. Radojevic, Comput. Phys. Commun. **18**, 87 (1979).
[13] D. J. Thouless, *The Quantum Mechanics of Many-Body Systems* (Academic, New York, 1972).
[14] I. Bray, D. V. Fursa, A. S. Kheifets, and A. T. Stelbovics, J. Phys. B **35**, R117 (2002).
[15] V. S. Yakovlev, J. Gagnon, N. Karpowicz, and F. Krausz, Phys. Rev. Lett. **105**, 073001 (2010).
[16] N. A. Cherepkov and S. K. Semenov, J. Phys. B **37**, 1267 (2004).